machines

MDPI

Article

Gyroid Lattice Heat Exchangers: Comparative Analysis on Thermo-Fluid Dynamic Performances

Ludovico Dassi, Steven Chatterton *, Paolo Parenti and Paolo Pennacchi

Department of Mechanical Engineering, Politecnico di Milano, Via La Masa 1, 20156 Milano, Italy; ludovico.dassi@polimi.it (L.D.); paolo.parenti@polimi.it (P.P.); paolo.pennacchi@polimi.it (P.P.)
* Correspondence: steven.chatterton@polimi.it

Abstract: In recent years, additive manufacturing has reached the required reliability to effectively compete with standard production techniques of mechanical components. In particular, the geometrical freedom enabled by innovative manufacturing techniques has revolutionized the design trends for compact heat exchangers. Bioinspired structures, such as the gyroid lattice, have relevant mechanical and heat exchange properties for their light weight and increased heat exchange area, which also promotes the turbulent regime of the coolant. This work focuses its attention on the effect of the relevant design parameters of the gyroid lattice on heat exchange performances. A numerical comparative analysis is carried out from the thermal and fluid dynamic points of view to give design guidelines. The results of numerical analyses, performed on cylindrical samples, are compared to the experimental results on the pressure drop. Lattices samples were successfully printed with material extrusion, which is a low-cost and easy-to-use metal AM technology. For each lattice sample, counter pressure, heat exchange, and turbulence intensity ratio are calculated from the numerical point of view and discussed. At the end, the gyroid lattice is proven to be very effective at enhancing the heat exchange in cylindrical pipes. Guidelines are given about the choice of the best lattice, depending on the considered applications.

Keywords: metal 3D printing; bioinspired heat exchanger; gyroid lattice; printed-circuit-heat-exchangers; heat transfer enhancement

Citation: Dassi, L.; Chatterton, S.; Parenti, P.; Pennacchi, P. Gyroid Lattice Heat Exchangers: Comparative Analysis on Thermo-Fluid Dynamic Performances. *Machines* **2024**, *12*, 922. https://doi.org/10.3390/machines12120922

Academic Editor: Sheng Li

Received: 6 November 2024
Revised: 9 December 2024
Accepted: 13 December 2024
Published: 16 December 2024

1. Introduction

In recent years, there has been growing interest in using additive manufacturing (AM) to incorporate bioinspired architectures into common heat exchangers [1–3]. This allows for more compact and lightweight components, increasing the heat transfer area and improving the mechanical resistance, as highlighted in [4,5]. The new generation of heat exchangers, characterized by high heat transfer efficiency and small dimensions, is known as the Printed Circuit Heat Exchanger (PCHE) [6]. This exchanger has found applications in various fields, including automotive, aerospace, and green energy production [7]. AM is an innovative production technique that relies on the gradual and localized addition of material to shape the final part. Material is added in layers, using various techniques such as binder printing or laser melting, depending on the material being processed [8,9]. These new production techniques have achieved significant reliability and defect management [10,11], becoming reliable alternatives to standard production techniques, which typically involve material removal. One of the most important advantages of AM is the significant geometrical freedom it offers in component design [12,13]. Specifically, it enables the creation of highly complex and interlocking geometries while maintaining lower production costs compared to traditional methods [14]. The use of bioinspired natural geometries has proven to be highly effective in enhancing the mechanical and thermal performance of conventional components [15,16]. Although many numerical studies have explored these geometries, they were nearly impossible to produce with standard manufacturing techniques [17]. A

representative example of a compact 3D-printed heat exchanger is presented in [18]. In the current study, the authors aim to investigate in detail the fluid dynamic performance of heat exchangers, specifically those needed for the oil-lubricated bearings of large rotating machines, as discussed by the same authors in [19].

In a previous work by Peng [20], the gyroid lattice was identified as one of the most promising geometries among known natural structures. The research trend has been confirmed by many recent works, such as [21]. This geometry was first discovered by biologist Alan Schoen in 1970 while studying the wing microstructure of C. Rubi butterflies [22,23]. From a mathematical perspective, the gyroid lattice is formalized as a triple periodic minimal surface (TPMS). In other words, given a specified boundary, the gyroid is the continuous surface that minimizes the total area and is periodic in space. The 3D surface can be modeled by the following equation:

$$\Phi(x,y,z) = \cos(x)\sin(y) + \cos(y)\sin(z) + \cos(z)\sin(x) = 0 \quad (1)$$

where (x, y, z) are the Cartesian coordinates. A key characteristic of the gyroid surface is its ability to divide space into two separate and continuously enveloped domains, significantly increasing the surface area for heat transfer and sustaining the turbulence regime of the coolant, as discussed in [24]. Once the minimal surface is defined, the 3D lattice can be created in two ways: by thickening the surface wall (sheet topology) or by solidifying one of the two domains (solid topology), as shown in Figure 1. The resulting lattices differ considerably from a fluid dynamic perspective, and they need further investigation. Three parameters must be defined to fully characterize the lattice structure: the lattice type (sheet or solid), the cell length (which is the dimension of the minimum repeatable cell), and the relative density (which is the ratio between the volume of the lattice and the volume of the bulk material).

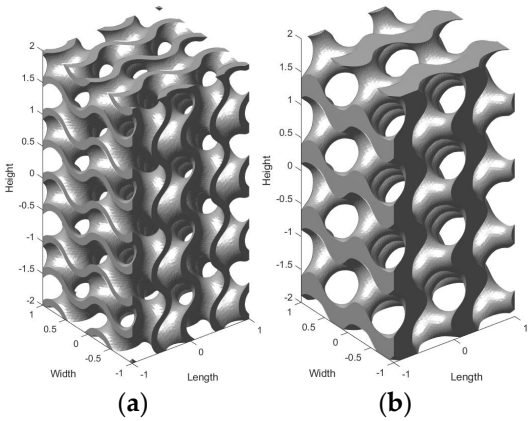

(**a**) (**b**)

Figure 1. Representative 3D models of gyroid lattice. (**a**) Sheet type with relative density 35%; (**b**) solid type with relative density 35%.

The existing literature contains numerous studies comparing the mechanical and thermal performance of various bioinspired microstructures, such as gyroid, diamond, octet-truss, and Schwartz-D lattices. All the authors agree that the gyroid lattice has notable mechanical properties due to its lightweight nature [25–27], and it guarantees the highest heat exchange when all other variables are held constant [24]. Notably, Koneri et al. [28] established a reliable procedure for quantifying and comparing the heat transfer properties of lattice geometries. They considered a circular pipe filled with the lattice geometries of interest, where heat flows from the hot walls to the coolant fluid. By imposing the coolant flow rate and the temperature of the external walls, several numerical fluid dynamic analyses were performed on the specimens. They found that the gyroid lattice can increase heat exchange by 50% compared to a plain cylindrical tube. This finding highlights the significant potential of the gyroid structure; however, there has been no investigation into

how the design parameters of the lattice affect the fluid dynamic performance of the heat exchanger. This work aims to fill that knowledge gap.

Another important aspect to consider is that the gyroid lattice has the critical but beneficial property of self-sustainability during the manufacturing process. In other words, it can be easily printed layer by layer with additive manufacturing techniques without requiring external supports to bear its self-weight. This feature facilitates the integration of the gyroid lattice into components without particular constraints, as discussed by Parenti in [29]. For manufacturing the samples, bound metal deposition (BMD) technology, an industrial implementation of the material extrusion process for metals, was chosen [30,31]. This innovative technique, based on metal-polymer feedstock extrusion and sintering, offers several advantages, such as powder-less printing (the feedstock filament is directly printed without the need for a powder bed [32]). This eliminates the challenging task of removing residual powder from internal channels. Additionally, it is a low-cost and easy-to-use technique that allows the printing of different metals, including stainless steel and copper, which are widely used in heat exchangers. Moreover this technology is widely investigated to increase the final printing quality, as discussed in [33].

The primary objective of this work is to compare the fluid dynamic properties of different gyroid lattices to provide insights for designing innovative bioinspired heat exchangers. The gyroid lattice is selected as the inner geometry, and a sensitivity analysis of key design parameters is developed and discussed. For the numerical analysis, the authors draw inspiration from the set-up described in [28] and use it to characterize different gyroid lattice geometries. The focus is on three fluid dynamic properties: the pressure drop required for coolant circulation, the turbulence intensity ratio, and the heat exchanged by the fluid. An experimental validation is then performed. The lattice samples are printed using BMD technology, inspected for printing defects, and flushed with oil and water to validate the numerical model on the pressure drop. The lattice material used is either stainless steel or copper. Although the choice of solid materials and coolant fluids is related to their final application in oil-lubricated bearings, the results are of general interest.

The paper is organized as follows. Section 2 describes the numerical model for predicting the fluid dynamic properties of gyroid lattice types. Section 3 presents the most relevant results of the numerical model. Section 4 focuses on the heat exchanged through conduction in the lattice walls and how this affects overall performance. Section 5 outlines the procedure for metal 3D printing of the samples and the experimental set-up. Section 6 presents the results of experimental flushing and the validation of the numerical model for pressure drop. Finally, Section 7 discusses the results and conclusions of the comparative analysis. It also mentions a possible practical application of the considered topic, performed by the same authors in [19].

2. Set-Up of Numerical Model for Fluid Dynamics

The analysis of the fluid dynamic properties of the gyroid lattice is performed by properly defining a computational fluid dynamics (CFD) model. The numerical simulations were performed using the software ANSYS Fluent, version 2021 R2. The simulations were performed under the hypothesis of steady-state conditions and an incompressible fluid. The thermal properties of the lubricant are a function of the local temperature.

In order to create the model geometry, the gyroid lattice is firstly defined by means of the tool “MS Lattice”, developed by Al-Ketan [25]. Then, the lattice geometry undergoes Boolean operations to create the liquid volume domain and the solid walls, as shown in Figure 2.

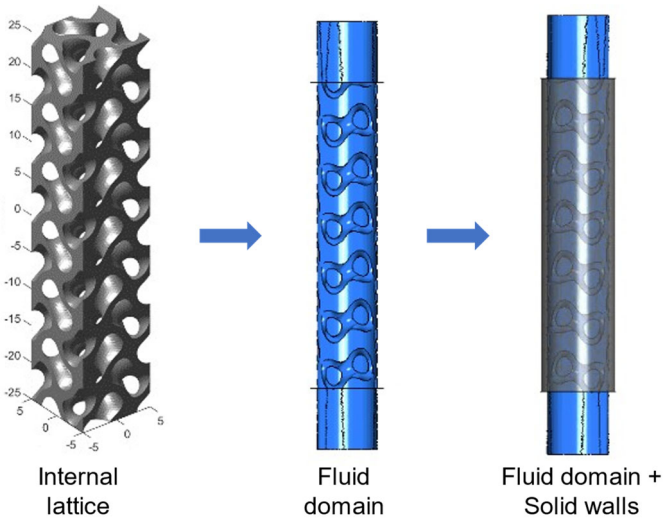

Figure 2. Boolean operations for the definition of the geometry of cylindrical samples filled with gyroid lattice structure. Both fluid and solid domains are present.

The procedure to quantify the heat exchange performance for different printed lattices is widely discussed by Koneri et al. in [28]. For the current study, the production steps are kept while the effective tube geometry is adapted to the current study. The representative sections of the heat exchanger have a cylindrical shape. The tubes have the following relevant dimensions: inner diameter is 10 mm, outer diameter is 14 mm, and tube length is 50 mm. Dimensions are chosen by considering interesting practical values and the printability capabilities of the available technology; nevertheless, the obtained results are useful for a comparative analysis and they are almost independent from the absolute dimensions. The tubes are filled with the gyroid lattice, and the design parameters are ranged. By considering the constraints for a reasonable design and to guarantee the printability, six lattice types are considered in the analysis with the following features: cell length = 8 mm is fixed, both sheet and solid topologies are considered, and relative density ranges between 15 and 45%. Cell length is chosen so that the minimum wall thickness in all the lattice domain is greater than 0.5 mm to guarantee printability. Other values of relative density are not considered since they will likely lead to excessively high pressure drop values or low heat exchange. Table 1 summarizes the six geometries under consideration. A schematic representation of the resulting domain is shown in Figure 3. The domains of interest are the solid part and the fluid one, calculated by Boolean operations.

Table 1. List of tube specimens considered for the analysis; different gyroid lattice geometries are addressed.

Specimen	Gyroid Type	Relative Density
1	Sheet	35%
2	Sheet	45%
3	Solid	15%
4	Solid	25%
5	Solid	35%
6	Solid	45%

The considered material for the solid part is AISI-316L steel or copper, while the fluid domain is filled with ISOVG68 oil or water. The choice of the materials results from a study by the same authors of a practical case, widely discussed in [19]. When oil is used, the numerical model should consider also the change in oil density and dynamic viscosity with respect to temperature, as shown in Figure 4.

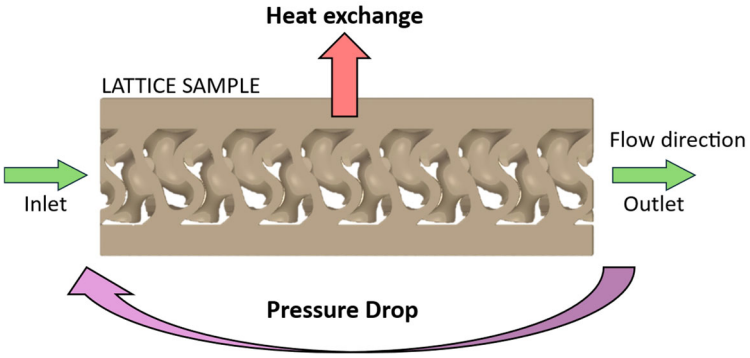

Figure 3. Schematic representation of the sample geometry and the thermal-fluid quantities of interest (pressure drop and heat exchange).

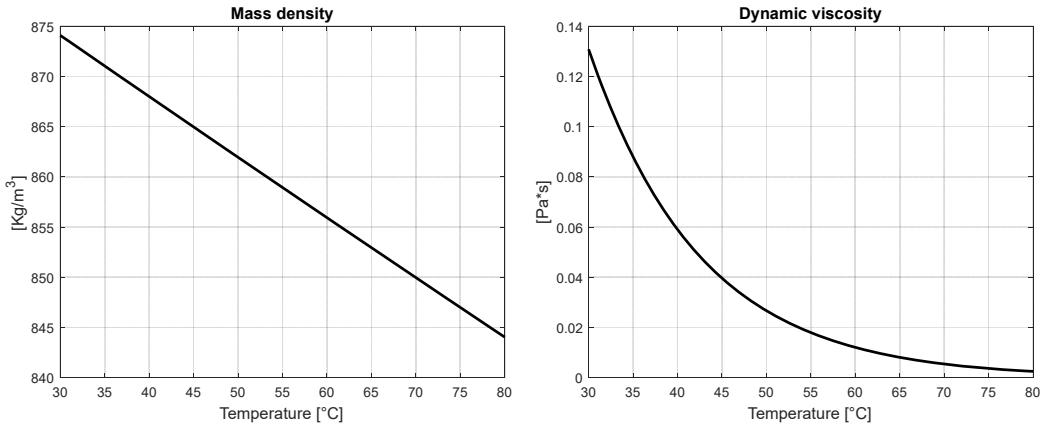

(**a**) (**b**)

Figure 4. Physical properties of the lubricant oil ISOVG68 as a function of temperature, (**a**) mass density, (**b**) dynamic viscosity.

The boundary conditions (BCs) applied to the domain are imposed as done in [28]; moreover, the used BCs can be easily reproduced during the experimental activities. Relevant surfaces are divided as shown in Figure 5; in particular, flow rate is imposed at the inlet and atmospheric pressure at the outlet of the duct. For the heat exchange, temperature is imposed at the coolant entrance (40 °C) and on the outer skin surface (60 °C). All the not-mentioned walls are considered adiabatic. All the boundary conditions are summarized in Table 2. Additional considerations must be made regarding wall roughness in additive manufacturing (AM) circuits. As stated by Hartsfield in [34], estimating the flow characteristics of AM parts can be challenging. For the components analyzed in this study, the nominal geometry of the walls was used, with an average surface roughness of 22 µm derived from experimental measurements on the printed parts. No significant model issues were observed, due to the short and straightforward geometry of the channels.

Table 2. List of thermal and fluid dynamic boundary conditions used in the simulations.

Surface Name	Description	BC Type
Inlet	Coolant entrance	Flow rate, 40 °C
Outlet	Coolant exit	Atmospheric pressure
Outer skin	Heated surface	Imposed temperature, 60 °C
Adiabatic walls	Not relevant walls	Adiabatic condition

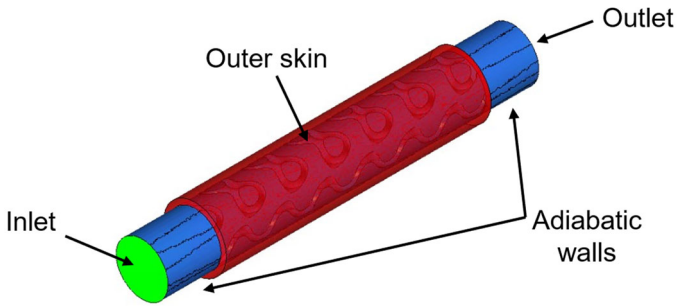

Figure 5. Schematics of the thermal and fluid dynamic boundary conditions used for the set-up of the numerical model.

The domain is divided with an unstructured tetrahedral mesh, edge size is approximately 0.25 mm, and total mesh is around 3.0 million elements. Local refinement is used in order to properly catch the geometry, and the inflation algorithm guarantees a good convergence of the solution on the wall boundary layer. Domain discretization is shown in Figure 6.

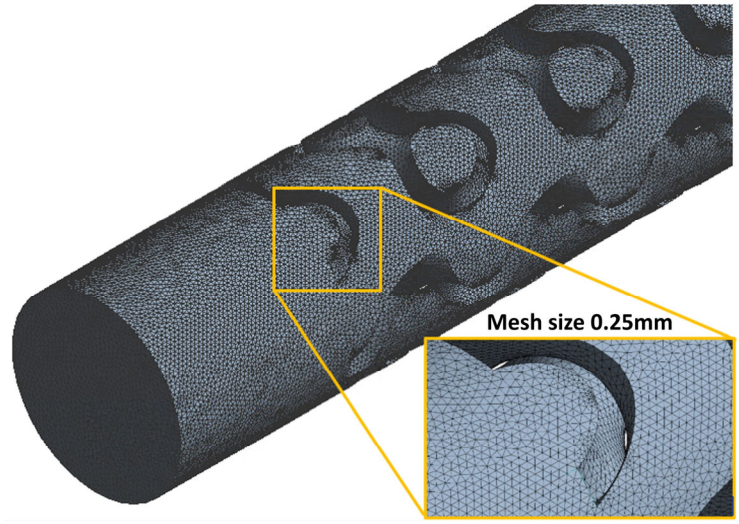

Figure 6. Volume discretization used for the numerical model and magnification of the boundary layer refinement.

The Reynolds-averaged Navier–Stokes equations are solved by means of a pressure-based solver and k-ω SST turbulence model, as commonly done in this field. Grid convergence index (GCI) analysis is performed to check for numerical convergence. Cell length is reduced up to 0.25 mm (3.0 M elements) to reach the asymptotical trend of the results. The convergence is checked for the following quantities of interest, namely the pressure drop between the inlet and the outlet of the duct, and the integral heat exchanged by the outer skin surface, as shown in Figure 7a. The residuals of the simulation are checked, and they ensure good convergence (relative error 10^{-6}). Moreover, the y+ value is checked at solid walls to be lower than unity, as proof of boundary layer correct modeling, as shown in Figure 7b. The convergence analysis is repeated for all the simulations. Once the model is correctly set up, simulations are repeated by changing the coolant type (oil/water) and the flow rate of the coolant (1–6 L/min). For each configuration, the pressure drop, heat flux, and turbulence motion of the flow regime (measured by the turbulence intensity ratio) are calculated.

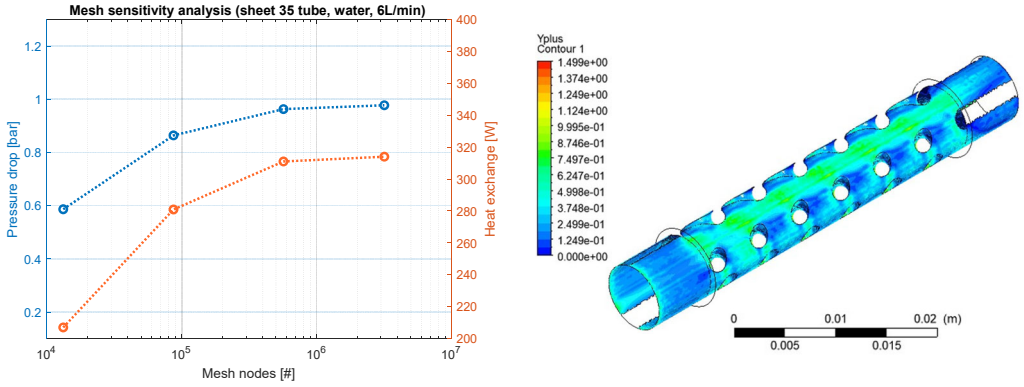

(**a**) (**b**)

Figure 7. Numerical convergence for the fluid dynamic analysis, tube with gyroid lattice, sheet type, relative density 35%, water coolant at 6 L/min. (**a**) Pressure drop and heat exchange sensitivity analysis with respect to mesh size; (**b**) plot of y+ value at solid walls.

3. Results of Numerical Model

The pressure drop, heat exchange, and turbulence intensity ratio are reported for each lattice type and for both fluids. When oil is used as a coolant, the maximum pressure drop reaches 3.63 bar, with a heat exchange of 135 W. In contrast, water proves to be a much more efficient coolant: the maximum pressure drop decreases to 1.24 bar, while heat exchange rises to 322 W (Figure 8a,b). Both the maximum heat exchange and maximum pressure drop occur with the 45% sheet lattice. However, the main drawback of sheet-type lattices is the high pressure drop they require. The relationship between pressure drop and relative density follows a direct quadratic trend. Heat exchange increases by 3 to 5 times when changing from a plain tube to a gyroid lattice, with the highest values found in sheet-type lattices. However, the relationship between heat exchange and relative density remains unclear. The numerical model presented in this work is experimentally validated for the pressure drop data, with the details of the validation process and results discussed comprehensively in Section 6. Appendix A gathers interesting resulting plots from the CFD analysis conducted on the different geometries with ISOVG68 oil as the coolant.

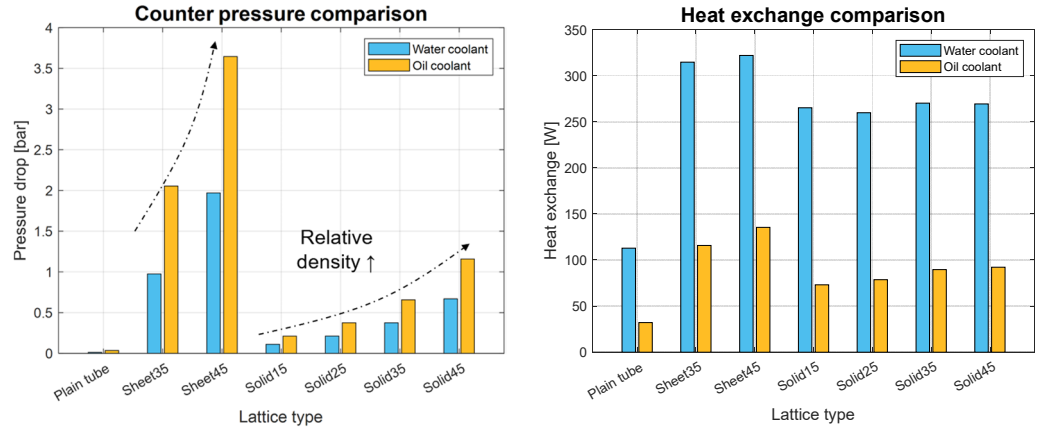

(**a**) (**b**)

Figure 8. Numerical results on different gyroid lattice samples, water and oil as coolant, flow rate 6 L/min, AISI-316L steel for solid walls. (**a**) Pressure drop values across the samples; (**b**) heat exchanged between coolant fluid and the outer cylindrical wall. Sheet lattice types maximize heat exchange and the required pressure drop.

Figure 9a shows the heat flux computed at the outer skin surface. The uneven distribution is caused by the lattice walls. Heat flux is higher where walls are connected to the outer skin. An interesting way to consider, at the same time, both heat exchange and backpressure terms is the so-called overall enhancement factor (*OEF*) [28], which is used to compare the efficiency of different heat exchanger geometries. From the mathematical point of view, it is the ratio between the percentual increase in heat exchange (Q) over the percentual increase in pressure drop (ΔP). The base case is a plain cylindrical tube (ΔP_0, Q_0).

$$OEF = \frac{Q/Q_0}{\Delta P/\Delta P_0} \tag{2}$$

where *OEF* is the overall enhancement Factor, Q and ΔP are the heat exchange and the pressure drop of the considered gyroid lattice sample, while Q_0 and ΔP_0 are the heat exchange and the pressure drop for the base case of the plain cylindrical tube.

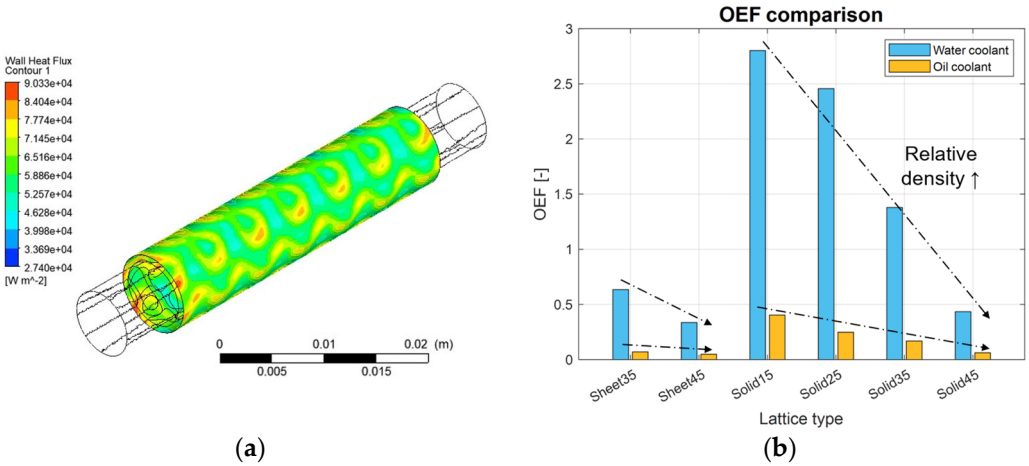

(**a**) (**b**)

Figure 9. Results of heat transfer from the numerical simulations. (**a**) Representative plot of heat flux over the outer skin surface; (**b**) comparative analysis on gyroid lattices with flow rate 6 L/min; solid-type lattices show higher values of overall enhancement factor.

Figure 9b shows that solid-type lattices have the highest overall efficiency factor, which is desirable as it indicates more heat exchange for a given pressure drop. Additionally, the relationship between relative density and the OEF appears to be nearly inversely linear within the relative density range of 15% to 45%. Under the same conditions, the 45% sheet lattice provides the highest heat exchange and pressure drop, while the 15% solid lattice offers the greatest efficiency, as indicated by the OEF. Lastly, water significantly improves performance compared to oil.

Furthermore, it is interesting to consider the turbulence intensity ratio (TI). It is a useful indicator to estimate the fluid regime of the coolant, it usually ranges in the interval TI $\in$ [0–40]% where the lowest values are related to the laminar motion, while the highest ones are related to the turbulent regime. In heat exchangers, turbulent motion is very useful because it significantly increases the heat exchanged on a given area. As shown in Figure 10, the gyroid lattice exhibits turbulent motion when water is used (average TI $\approx$ 20%); in contrast, oil is too viscous and the motion is still laminar when it is used (average TI $\approx$ 0%). Values higher than 50% should not be considered, since they are the result of the intricate geometry of the lattice and the kinematic calculation of the TI.

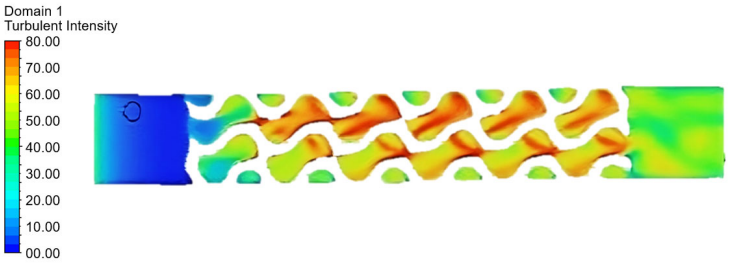

Figure 10. Numerical simulation of the flow in gyroid lattice sample, sheet type, relative density 35%, water as coolant, flow rate 6 L/min. Plot of the turbulence intensity ratio (TI) along longitudinal plane.

4. Study of Heat Exchange in Solid Lattice

For the considered case, the heat flux is exchanged between the outer cylindrical wall of the tube and the coolant fluid. For this set-up, the heat exchange capability is governed by two phenomena:

- Fluid-to-solid convection between coolant fluid and lattice walls;
- Solid-to-solid conduction inside solid walls of the lattice.

In this section, fluid convection is kept fixed and heat conduction in lattice walls is investigated. It is important to note that, according to the existing literature, the gyroid lattice can be used in two distinct ways. The most common application involves exchanging heat between two different fluids, where the two domains of the gyroid lattice remain well separated, and heat transfers between the two fluids through the thin walls of the lattice. On the other hand, the current study focuses on heat exchange between a hot outer wall and a coolant fluid that fills all the fluid domains of the gyroid lattice. In this scenario, the gyroid lattice functions similarly to a finned geometry, increasing the surface area between the fluid and solid domains. As studied by Tao et al. in [35], thermal conductivity in solids becomes a key aspect for small fins because it affects temperature distribution along the fin itself, as shown in the scheme of Figure 11. For a heat-dissipating fin, the longitudinal temperature distribution results from the thermal balance between conduction and convection. As a result, the average temperature is directly proportional to the conduction coefficient.

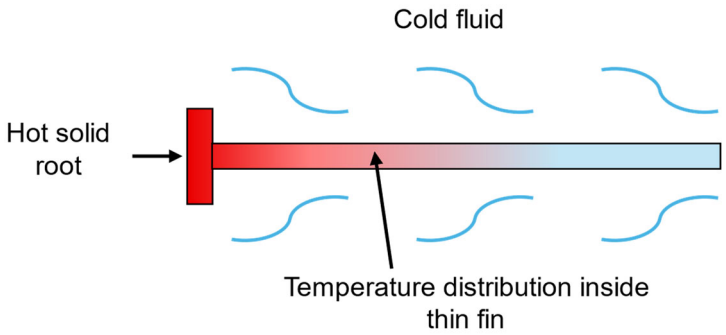

Figure 11. Qualitative sketch of temperature trend along a cooled thin fin.

Therefore, the higher the average temperature of the fin, the greater the heat exchange.

In the literature, this problem is typically analyzed using an ideal reference case known as "isothermal fin". In this scenario, the entire finned region is assumed to have the same temperature as the base material, maximizing convective heat transfer due to the large temperature difference between the cold fluid and the hot fin surface. However, in real-world conditions, the temperature distribution in the fin is heavily influenced by the material thermal conductivity. Materials with higher thermal conductivity, such as copper or aluminum, increase the average temperature of the fin, enhancing heat transfer efficiency. The fin conduction efficiency is defined as the ratio between the actual heat flux and the maximum possible heat flux in the isothermal fin case.

To apply this concept to a gyroid lattice structure, dedicated numerical simulations were conducted. The solid domain is now added to the fluid dynamic analysis. A coarser mesh is used to solve the heat conduction equation inside the solid material. The case of interest involves a sheet-type gyroid lattice with relative density 35% and a flow rate of 6 L/min, considering both ISOVG68 oil and water as working fluids. For each fluid, the flow conditions remain constant, while the thermal properties of the solid material vary. The relent thermal properties of the materials are reported in Table 3.

Table 3. Thermal properties of the materials used for simulations.

Material	Density [kg/m^3]	Dynamic Viscosity [Pa·s]	Specific Heat [J/kg-K]	Thermal Conductivity [W/(m·K)]
Steel AISI-316L	8030	-	502	16.27
Copper	8978	-	381	387.60
Water	998	0.001	4182	0.60
Oil ISOVG68 (40 °C)	878	0.04	1934	0.15

Three scenarios are analyzed: in the first, the solid domain is maintained at a constant temperature equal to that of the hot outer surface, simulating an ideal isothermal fin. In the other two cases, the material of the solid domain is either copper or steel. For the last cases, the temperature at the outer surface is fixed, but the temperature distribution within the solid domain is determined by the balance of heat transfer. Consequently, the heat exchange will be lower.

By looking at the results in Table 4, it is important to assess the efficiency gain when changing the solid material relative to the ideal condition. The ideal isothermal case, by definition, always exhibits maximum efficiency. Notably, the efficiency difference between stainless steel and pure copper is approximately 43% for both oil and water cases. This consistent difference is due to the thermal resistance imposed by conduction in the solid material; copper is the favorable solution, even though more expensive. When looking at the coolant fluid, water is favorable with respect to oil. Although water exhibits lower heat exchange efficiency, which might seem counterintuitive, this is correct and can be explained by the increase in absolute heat exchange values. In other words, when water is used, lower efficiency means that the material choice for the solid domain becomes a bottleneck in heat exchange and it significantly reduces the overall exchanged heat. As a result of this analysis, copper is deemed the favorable choice, particularly when water is used as the coolant, resulting in higher heat exchange. The temperature fields computed for these calculations are shown in Figure 12, with a gyroid lattice, sheet type, relative density 35% and water flow rate of 6 L/min.

Table 4. Effect of solid material choice on heat exchange. Calculation of heat conduction efficiency in solid walls as a function on the solid material (AISI-316L or pure copper) and coolant fluid (ISOVG68 or pure water). Gyroid lattice, sheet type, relative density 35%, flow rate 6 L/min.

Coolant Fluid	Solid Material	Heat Flux [W]	Efficiency [%]
ISOVG68	AISI-316L	116	40%
	Pure copper	242	84%
	Ideal isothermal	287	100%
Water	AISI-316L	313	14%
	Pure copper	1260	56%
	Ideal isothermal	2240	100%

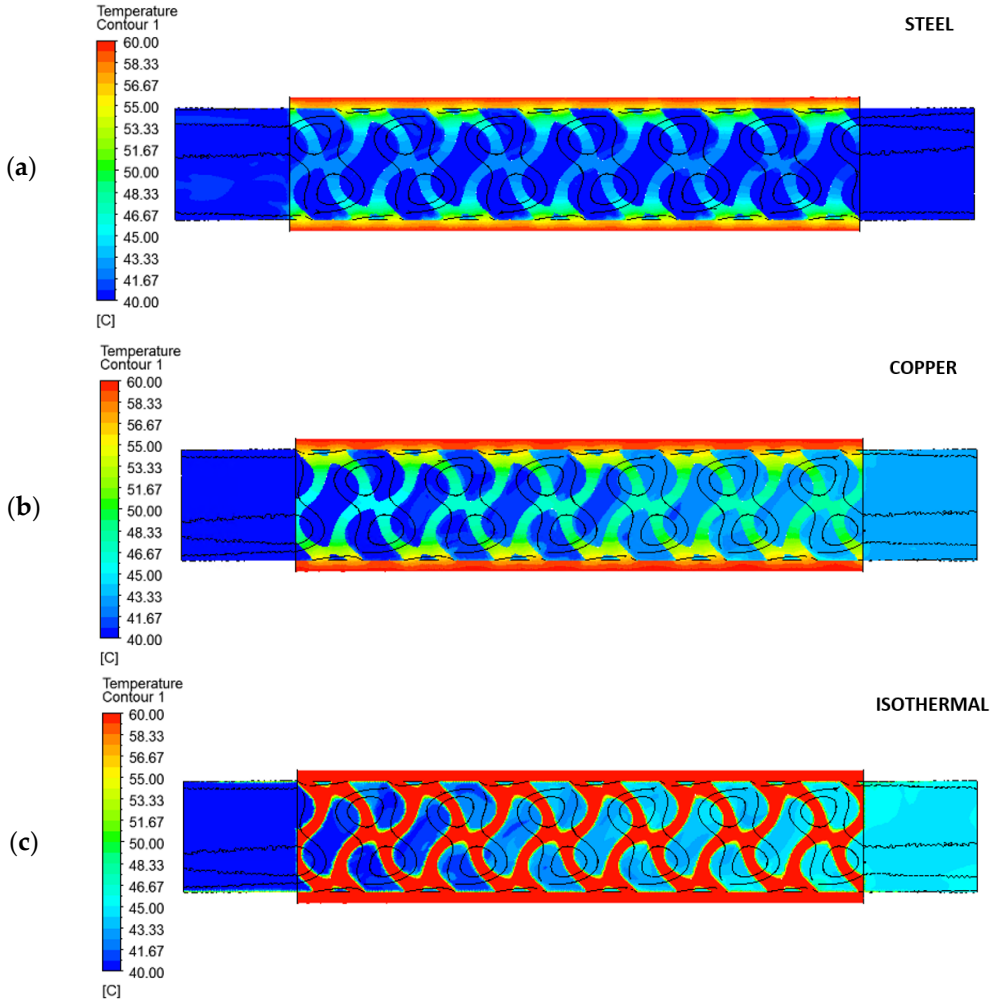

Figure 12. Temperature field for calculations on heat conduction in walls. Tube with gyroid lattice, sheet type, relative density 35%. Material for solid walls is: (**a**) stainless steel AISI-316L; (**b**) pure copper; (**c**) ideal case with isothermal solid walls.

5. Manufacturing of Samples and Set-Up of Experimental Campaign

In order to validate the numerical results, a complementary experimental campaign was performed to reproduce the results of the simulations. First of all, the samples were successfully printed with bound metal deposition technology (Figure 13), which consists of a material extrusion technique (MEX), in AISI-316L stainless steel [36–38]. The most important advantages of this technology are the ease of use and the absence of loose metal powder, which could be difficult to flush away from the internal cavities. Examples of the resulting tubes are shown in Figure 13. Gyroids have been proved to be printable with great accuracy, without the need of any internal supports.

After visual inspection, no evident geometrical defects and dimension errors were present.

CT scanning was conducted on one tube filled with a sheet-type gyroid lattice of 35% as shown in Figure 14a,b, to verify the consistency in the gyroid filling. A high-resolution microfocus CT system (300 kV Baker Hughes GE Phoenix V | tome | x) was employed for CT scans, featuring a microfocus X-ray. Equipped with a high-efficiency digital detector (e.g., flat-panel detector), the system employs advanced filtered back-projection algorithms for 3D image reconstruction. The adopted voxel resolution for the scan was 15 µm. The full video of the CT scan analysis is available in the Supplementary Materials.

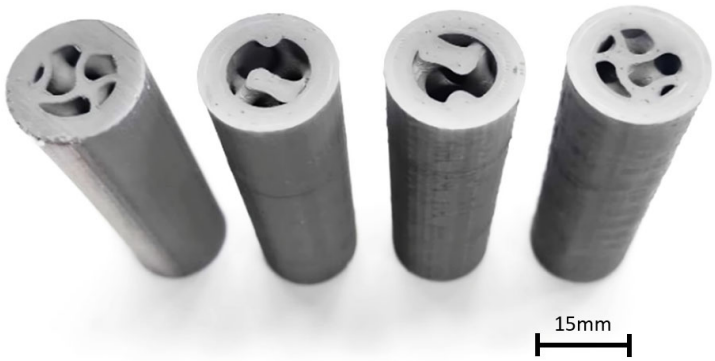

Figure 13. AISI-316L examples of cylindrical samples printed with BMD for the experimental campaign. Tubes are filled with a gyroid lattice, both solid and sheet types.

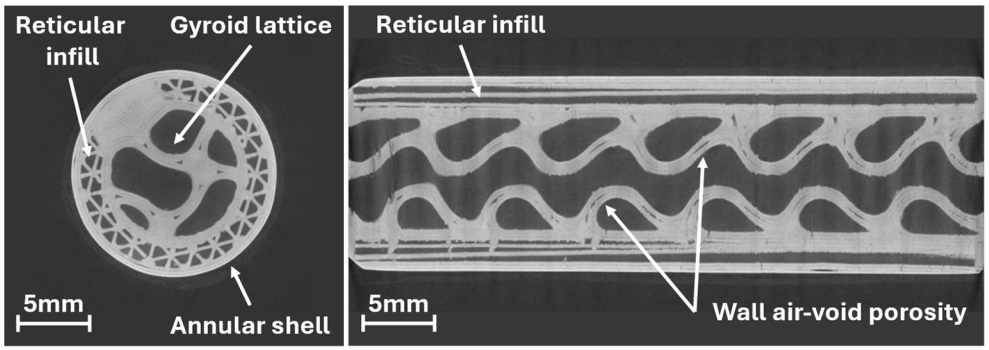

(**a**) (**b**)

Figure 14. CT scan of one printed cylindrical sample, filled with sheet-type gyroid lattice and relative density 35%. The internal geometry is free of relevant defects and distortions, even though examples of wall air void porosity are present inside the gyroid walls. Inside the cylindrical annular shell, it is possible to notice the reticular structure used to fill the outer wall. (**a**) Mid-height cross-section; (**b**) longitudinal section.

By looking at the results, the internal geometry appears correctly printed; no relevant defects are present, and no wall collapse is visible. Only localized and small air void porosity is noticed inside the gyroid walls, as a consequence of the 3D printing extrusion path adopted. Generally speaking, the scans confirm the successful printing of the components. Moreover, it is possible to notice the reticular structure (i.e., the infill) used inside the wall of the cylindrical annular shell.

Subsequently, printed lattice samples were tested on a dedicated flushing circuit, as shown in Figure 15a,b. The test bench is able to measure the pressure drop across the lattice sample. The type of coolant can be changed (oil or water), and the temperature and the flow rate of the coolant can be measured and adjusted. When oil is used, it is important to control the coolant temperature in order to guarantee the same viscosity used in simulations. The set-up is composed of an external pumping unit for the coolant with a temperature controller and a measuring apparatus. The temperature controller guarantees thermal steady-state conditions for the cooling fluid. The recirculation circuit is used before the measuring phase to easily reach a steady-state thermal condition. The coolant temperature and pressure drop across the sample are measured by probes, while the flow rate is calculated by weighing on a digital scale a certain quantity of coolant and the time needed to flow. Pressure measurements are performed for each coolant (oil/water) by adjusting the flow rate (1–6 L/min). Each measurement is repeated five times for robustness. The main limitation of the apparatus is its inability to measure heat exchange due to technical constraints. The main challenge lies in accurately controlling the outer wall temperature of the tube, which is critical for reliable heat transfer measurements. This

typically requires an isothermal, temperature-controlled chamber. However, such a system is usually expensive and complex.

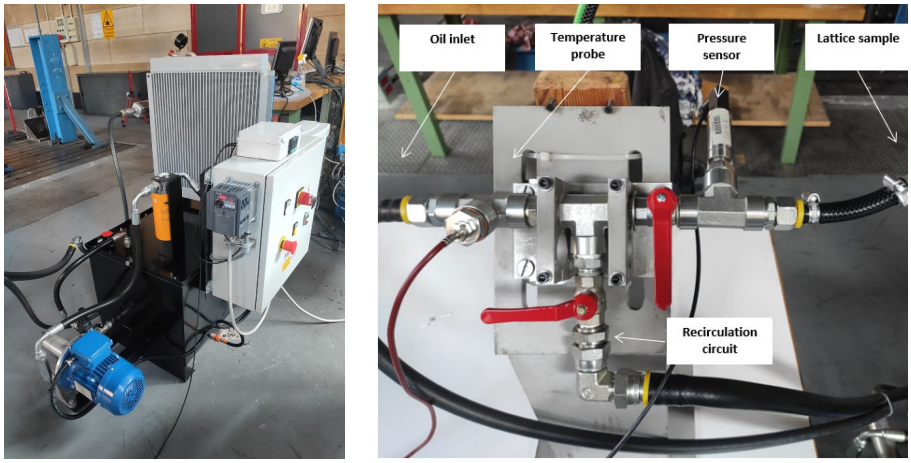

(**a**) (**b**)

Figure 15. Flushing circuit for experimental measurements on the printed lattice samples. (**a**) Pumping unit with temperature controller; (**b**) manifold for flushing of the samples.

6. Experimental Results and Model Validation for Pressure Drop

Experimental pressure data are analyzed in this section. Pressure curves as a function of coolant flow rate are calculated for each sample and coolant type, as illustrated in Figure 16a. The experimental data are accurately interpolated using a second-order polynomial, with a high correlation coefficient of 99.7%, confirming the absence of significant disturbance effects during the experiments. The choice of a second-order polynomial is based on the Bernoulli equation and is not linked to the numerical analysis.

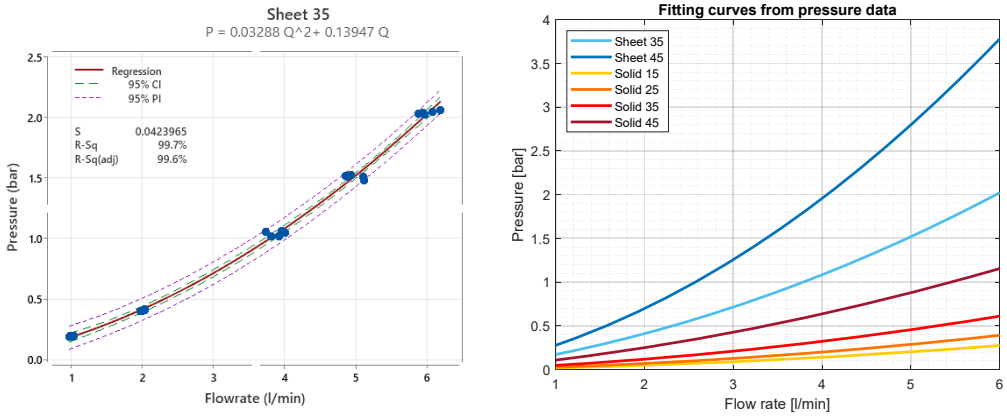

(**a**) (**b**)

Figure 16. Pressure curves from experimental measurements on lattice samples flushed with oil. (**a**) Measurement data points and fitting curve for gyroid lattice, sheet type, relative density 35%, flow rate 1–6 L/min; (**b**) fitting curves for all the specimens.

Regarding the uncertainty analysis for the pressure curves, the uncertainty in flow rate is ±0.3%, while the uncertainty in pressure is ±0.1%. This procedure is applied to all tubes, and the resulting interpolated curves for oil are shown in Figure 16b.

The experimental flushing was useful for validating the numerical model. The comparison between the experimental and the numerical data on the pressure drop is reported in Figure 17. The difference is expressed as the average relative error on the pressure drop, for each lattice sample. The following equation was used to define the relative difference in the pressure drop:

$$err = \frac{\Delta P_{exp} - \Delta P_{num}}{\Delta P_{num}} \times 100 \quad (3)$$

where err is the percentual difference between the measurements, ΔP_{exp} is the experimental measurement of the pressure drop, and ΔP_{num} is the numerical estimation of the pressure drop. For the different flow rates and lattice samples, the average error is around 5% and is considered satisfactory, given the complexity of the studied geometry. The highest error occurs for the solid lattice with relative density of 15%, probably because of some internal printing defects. The developed model is proved to be accurate for the estimation of the pressure drop. Conversely, no validation can be performed on heat exchange values due to experimental set-up difficulties, as discussed in Section 5.

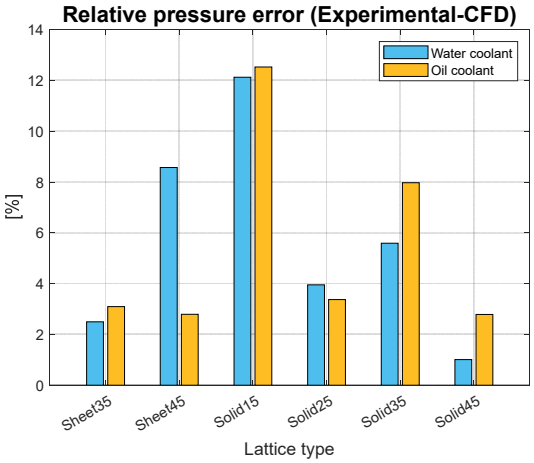

Figure 17. Mean pressure error between numerical and experimental data for the considered lattices, flow rate 6 L/min.

7. Discussion and Conclusions

The proposed research develops a numerical model for estimating the internal fluid dynamics in gyroid lattices. The model results align well with the experimental findings, providing confidence in the approach. Several key insights emerge from the study.

Firstly, as shown by the numerical results on pressure drop in Figure 8a, the gyroid lattice exhibits significantly higher backpressure compared to a plain tube. This outcome is expected due to the more complex fluid pathways within the lattice. In heat exchange applications, pumping power is typically several orders of magnitude lower than the heat exchanged, which often justifies neglecting it. However, it is common practice to set a maximum allowable backpressure that suits the specific application. In industrial contexts, pressures below 10 bars are generally manageable.

Regarding heat exchange performance (Figure 8b), the gyroid lattice significantly enhances heat transfer, achieving up to five times the baseline level. This result is crucial as it confirms findings from the existing literature. Additionally, it is noteworthy that the sheet lattice exhibits slightly higher heat transfer, approximately 20% more than the solid type, likely due to differences in the effective heat transfer area.

To effectively compare the performance of different lattices, it is essential to consider both the heat exchange and pressure drop contributions, using the overall enhancement

factor (Figure 9b). This metric clearly indicates the heat exchange efficiency, with solid lattices emerging as the more favorable option. Ultimately, the choice of lattice design should balance the required heat exchange with acceptable backpressure levels, depending on the specific application. For the case considered (solid-to-fluid heat exchange), conduction in the solid material is a critical factor and should be carefully considered in the final design. Highly conductive materials, such as copper or aluminum, are highly recommended when water coolant is used.

This experimental work has been particularly valuable in validating the proposed geometries. Additive manufacturing has demonstrated its capability to successfully produce the samples, with no significant defects observed, and the geometry showing excellent self-sustainability, as confirmed by the CT scan.

In conclusion, this research advances the current understanding of the heat transfer capabilities of gyroid lattices. The complex lattice geometry effectively promotes and sustains fluid turbulence, especially when water is used, leading to a substantial increase in heat exchange. A comparative analysis was conducted by varying key lattice design parameters, and the resulting pressure drop data were validated through a dedicated experimental campaign, showing good agreement. Additionally, an interesting industrial application of the gyroid lattice is detailed by the same author in [19]. A promising area for future work is the optimization of the external shape of the heat exchanger, where developing innovative topologies could further enhance cooling capabilities while reducing coolant backpressure.

Supplementary Materials: The following supporting information can be downloaded at: https://www.mdpi.com/article/10.3390/machines12120922/s1, Video S1: CT scan of sample gyroid sheet 35% cross-section plane, Video S2: CT scan of sample gyroid sheet 35% longitudinal plane.

Author Contributions: Conceptualization, L.D. and S.C.; methodology, L.D.; software ANSYS Fluent v2021R2, Matlab R2023b, Minitab v22, L.D.; validation, L.D and P.P. (Paolo Parenti); formal analysis, S.C.; investigation, L.D.; resources, P.P. (Paolo Pennacchi); data curation, L.D.; writing—original draft preparation, L.D.; writing—review and editing, S.C.; visualization, L.D.; supervision, P.P. (Paolo Parenti); project administration, P.P. (Paolo Pennacchi); funding acquisition, P.P. (Paolo Pennacchi). All authors have read and agreed to the published version of the manuscript.

Funding: This research was co-funded by "Italian Ministry for Education, University and Research" Ministry for Education, University and Research", project Department of Excellence LIS4.0 (Integrated Laboratory for Lightweight and Smart Structures, Grant number ID:D56C18000400006).

Data Availability Statement: The datasets presented in this article are not readily available due to technical limitations.

Conflicts of Interest: The authors declare no conflicts of interest.

Appendix A

Resulting plots from the CFD numerical analysis conducted on the different geometries with ISOVG68 oil as coolant. Velocity and temperature fields over the domain.

Plain tube, coolant: ISOVG68 oil, flow rate: 6 L/min.

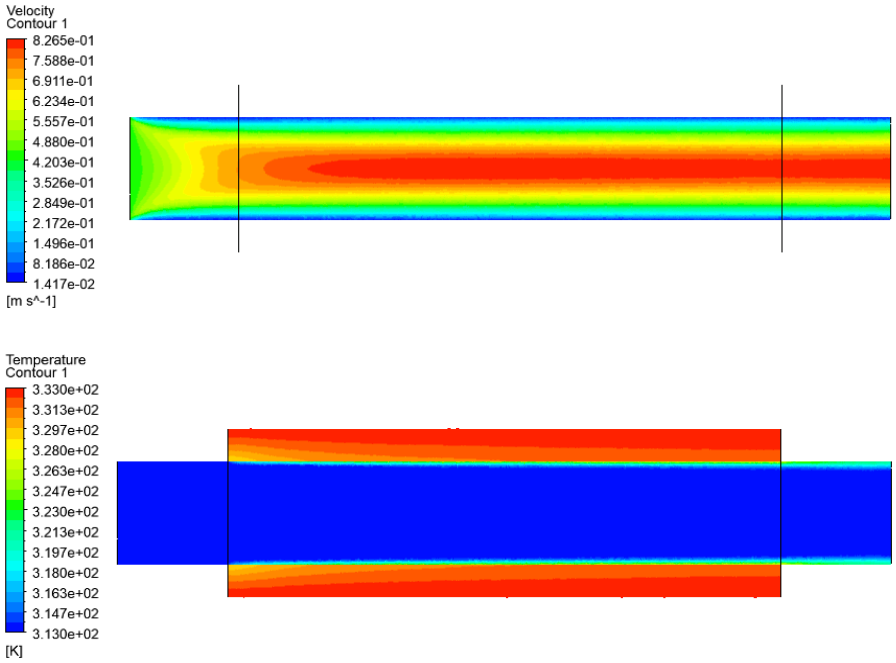

Gyroid lattice, sheet-based 35%, coolant: ISOVG68 oil, flow rate: 6 L/min.

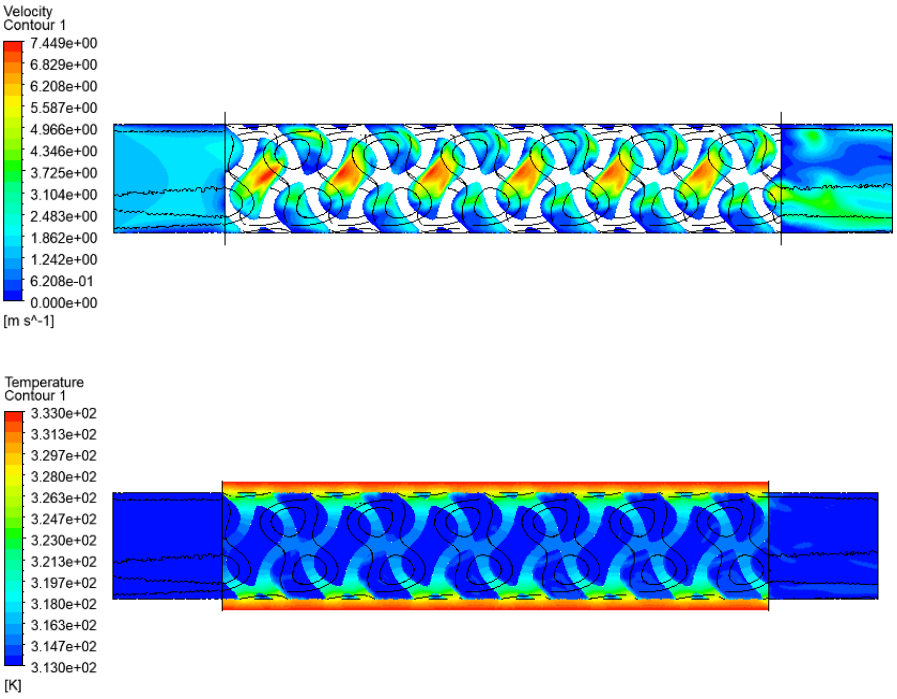

Gyroid lattice, sheet-based 45%, coolant: ISOVG68 oil, flow rate: 6 L/min.

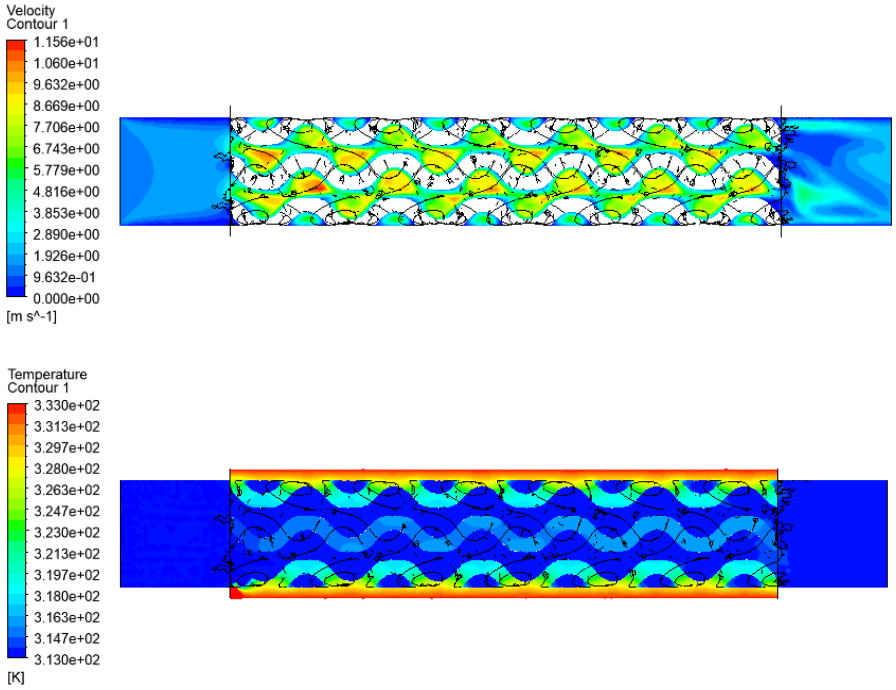

Gyroid lattice, solid-based 15%, coolant: ISOVG68 oil, flow rate: 6 L/min.

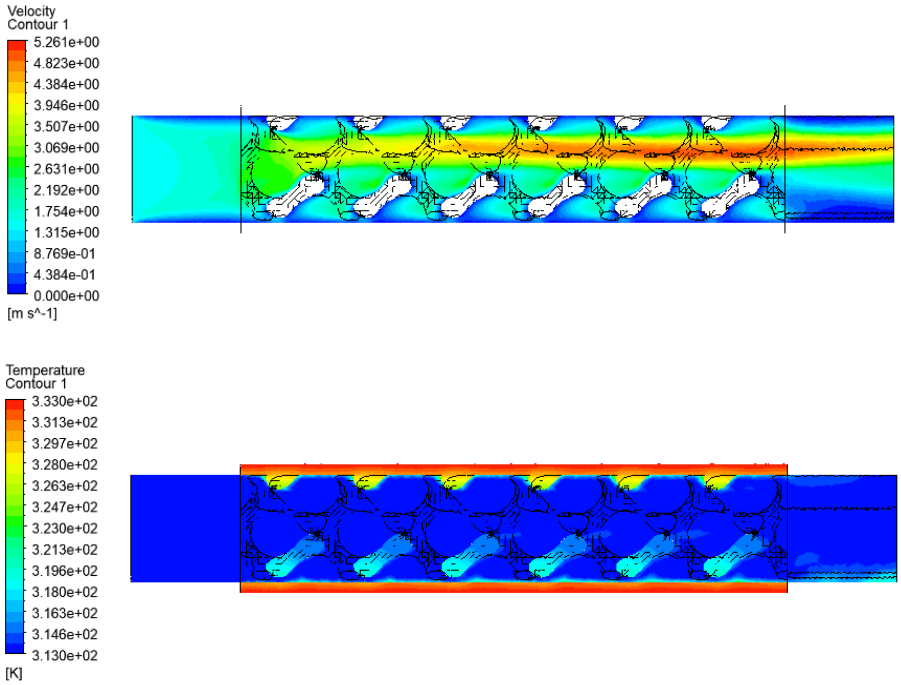

Gyroid lattice, solid-based 25%, coolant: ISOVG68 oil, flow rate: 6 L/min.

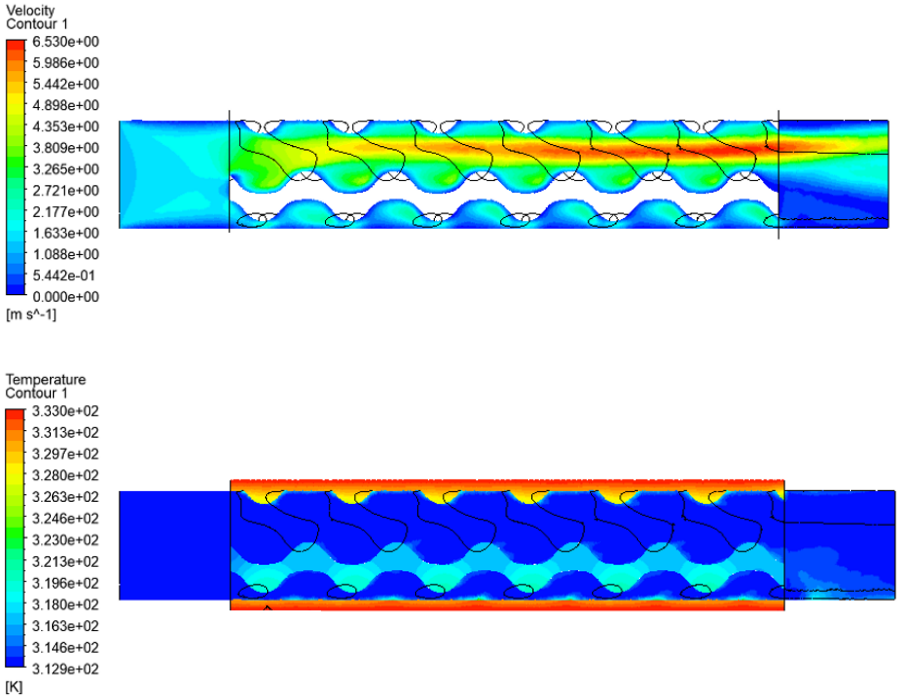

Gyroid lattice, solid-based 35%, coolant: ISOVG68 oil, flow rate: 6 L/min.

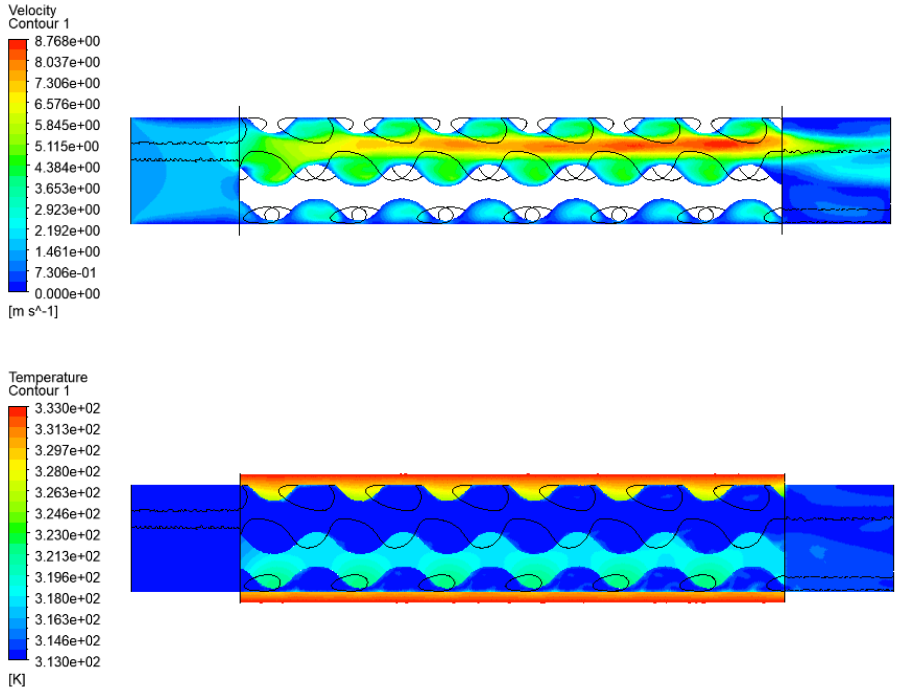

Gyroid lattice, solid-based 45%, coolant: ISOVG68 oil, flow rate: 6 L/min.

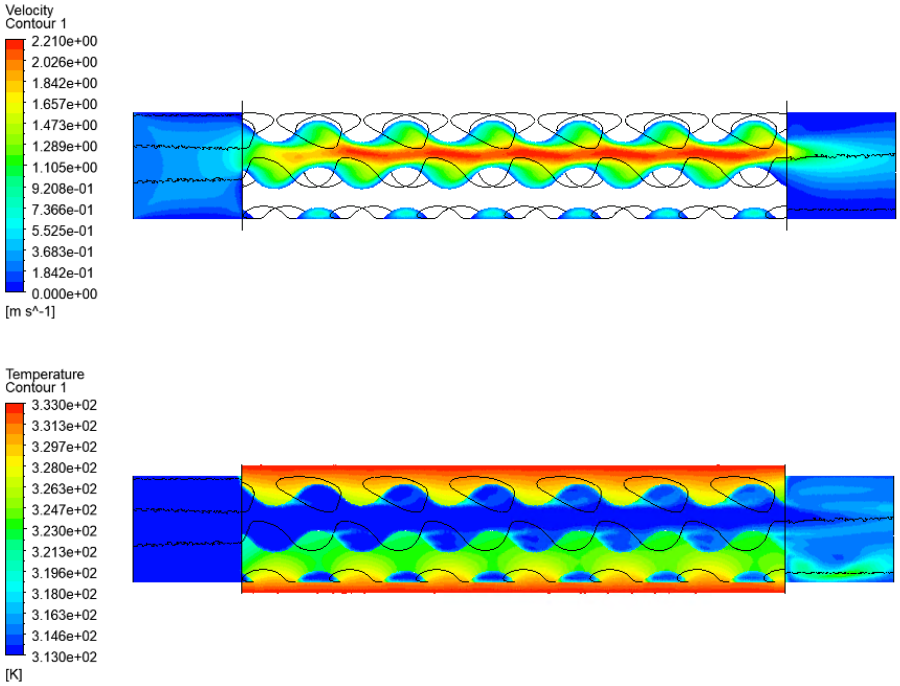

References

1. Kwon, O.-K. Heat Transfer and Pressure Drop Characteristics in Zigzag Channel Angles of Printed Circuit Heat Exchangers. *Korean J. Air-Cond. Refrig. Eng.* **2009**, *21*, 475–482.
2. Iyer, J.; Moore, T.; Nguyen, D.; Roy, P.; Stolaroff, J. Heat transfer and pressure drop characteristics of heat exchangers based on triply periodic minimal and periodic nodal surfaces. *Appl. Therm. Eng.* **2022**, *209*, 118192. [CrossRef]
3. Careri, F.; Khan, R.H.U.; Todd, C.; Attallah, M.M. Additive manufacturing of heat exchangers in aerospace applications: A review. *Appl. Therm. Eng.* **2023**, *235*, 121387. [CrossRef]
4. Liang, D.; Shi, C.; Li, W.; Chen, W.; Chyu, M.K. Design, flow characteristics and performance evaluation of bioinspired heat exchangers based on triply periodic minimal surfaces. *Int. J. Heat Mass Transf.* **2023**, *201*, 123620. [CrossRef]
5. Kaur, I.; Singh, P. State-of-the-art in heat exchanger additive manufacturing. *Int. J. Heat Mass Transf.* **2021**, *178*, 121600. [CrossRef]
6. Li, Q.; Zhan, Q.; Yu, S.; Sun, J.; Cai, W. Study on thermal-hydraulic performance of printed circuit heat exchangers with supercritical methane based on machine learning methods. *Energy* **2023**, *282*, 128711. [CrossRef]
7. Zhang, L.; Feih, S.; Daynes, S. Energy absorption characteristics of metallic triply periodic minimal surface sheet structures under compressive loading. *Addit. Manuf.* **2018**, *23*, 505–515. [CrossRef]
8. Rajaguru, K.; Karthikeyan, T.; Vijayan, V. Additive manufacturing—State of art. *Mater. Today Proc.* **2020**, *21*, 628–633. [CrossRef]
9. Rajendrachari, S. *Practical Implementations of Additive Manufacturing Technologies*, 1st ed.; Springer: Singapore, 2023; ISBN 978-981-9959-48-8.
10. Ye, H.; Liu, X.Y.; Hong, H. Fabrication of metal matrix composites by metal injection molding, A review. *J. Mater. Process. Technol.* **2008**, *200*, 12–24. [CrossRef]
11. Gibson, I.; Rosen, D.; Stucker, B. *Additive Manufacturing Technologies: 3D Printing, Rapid Prototyping, and Direct Digital Manufacturing*; Springer: Singapore, 2021; ISBN 978-3-030-56129-1.
12. Nsiempba, K.M.; Wang, M.; Vlasea, M. Geometrical Degrees of Freedom for Cellular Structures Generation: A New Classification Paradigm. *Appl. Sci.* **2021**, *11*, 3845. [CrossRef]
13. Fuchs, D.; Bartz, R.; Kuschmitz, S.; Vietor, T. Necessary advances in computer-aided design to leverage on additive manufacturing design freedom. *Int. J. Interact. Des. Manuf.* **2022**, *16*, 1633–1651. [CrossRef]
14. Hancock, D.; Homfray, D.; Porton, M.; Todd, I.; Wynne, B. Exploring complex high heat flux geometries for fusion applications enabled by additive manufacturing. *Fusion Eng. Des.* **2018**, *136*, 454–460. [CrossRef]
15. Hassan, I.M.; Enab, T.A.; Fouda, N.; Eldesouky, I. Design, fabrication, and evaluation of functionally graded triply periodic minimal surface structures fabricated by 3D printing. *J. Braz. Soc. Mech. Sci. Eng.* **2023**, *45*, 66. [CrossRef]
16. Mahmoud, D.; Tandel, S.R.S.; Yakout, M.; Elbestawi, M.; Mattiello, F.; Paradiso, S.; Ching, C.; Zaher, M.; Abdelnabi, M. Enhancement of heat exchanger performance using additive manufacturing of gyroid lattice structures. *Int. J. Adv. Manuf. Technol.* **2023**, *126*, 4021–4036. [CrossRef]
17. Sartini, M.; Bianchi, I.; Vita, A.; Germani, M.; Mandolini, M. An analytic cost model for bound metal deposition. *Proc. Des. Soc.* **2024**, *4*, 1819–1828. [CrossRef]

18. Vlahinos, M.; O'Hara, R. Unlock Breakthrough Heat Exchanger Designs with Gyroids | Ansys. 2022. Available online: https://www.ansys.com/blog/heat-exchanger-designs-gyroids (accessed on 1 September 2024).
19. Dassi, L.; Chatterton, S.; Parenti, P.; Vania, A.; Colosimo, B.M.; Pennacchi, P. Cooled pads with bioinspired gyroid lattice for tilting pad journal bearings: Experimental validation of numerical model for heat transfer. *Tribol. Int.* **2023**, *184*, 108448. [CrossRef]
20. Peng, H.; Gao, F.; Hu, W. Design, modelling and characterization of Triply Periodic Minimal Surface heat exchangers with Additive Manufacturing. In Proceedings of the Solid Freeform Fabrication Symposium, Austin, TX, USA, 12–14 August 2019.
21. Kus, K.; Wójcik, M.; Malecha, Z.; Rogala, Z. Numerical and experimental investigation of the gyroid heat exchanger. *Int. J. Heat Mass Transf.* **2024**, *231*, 125882. [CrossRef]
22. Schoen, A.H. Infinite Periodic Minimal Surfaces Without Self-Intersections. 1970. Available online: https://ntrs.nasa.gov/citations/19700020472 (accessed on 1 September 2024).
23. Michielsen, K.; Stavenga, D.G. Gyroid cuticular structures in butterfly wing scales: Biological photonic crystals. *J. R. Soc. Interface* **2008**, *5*, 85–94. [CrossRef]
24. Li, W.; Yu, G.; Yu, Z. Bioinspired heat exchangers based on triply periodic minimal surfaces for supercritical CO_2 cycles. *Appl. Therm. Eng.* **2020**, *179*, 115686. [CrossRef]
25. Al-Ketan, O.; Rezgui, R.; Rowshan, R. Microarchitected Stretching-Dominated Mechanical Metamaterials with Minimal Surface Topologies. *Adv. Eng. Mater.* **2018**, *20*, 1800029. [CrossRef]
26. Cao, X.; Yang, H.; Ren, X.; Wu, W.; Xi, L.; Li, Y.; Fang, D. Mechanical performance and defect analysis of the imperfect micro smooth gyroid cylinder shell structure. *Compos. Struct.* **2021**, *273*, 114320. [CrossRef]
27. Maharjan, G.K.; Khan, S.Z.; Riza, S.H.; Masood, S.H. Compressive Behaviour of 3D Printed Polymeric Gyroid Cellular Lattice Structure. *IOP Conf. Ser. Mater. Sci. Eng.* **2018**, *455*, 012047. [CrossRef]
28. Koneri, R.; Mulye, S.; Ananthakrishna, K. Additive Manufacturing of Lattice Structures for Heat Transfer Enhancement in Pipe Flow. In *Industry 4.0 and Advanced Manufacturing*; Lecture Notes in Mechanical Engineering; Springer: Singapore, 2021; pp. 233–246.
29. Parenti, P.; Puccio, D.; Colosimo, B.M. A new solution for assessing the printability of 17-4 PH gyroids produced via extrusion-based metal AM. *J. Manuf. Process.* **2022**, *74*, 557–572. [CrossRef]
30. Galantucci, L.M.; Pellegrini, A.; Guerra, M.G.; Lavecchia, F. 3D Printing of parts using metal extrusion: An overview of shaping debinding and sintering technology. *Adv. Technol. Mater.* **2022**, *47*. [CrossRef]
31. Sadaf, M.; Bragaglia, M.; Slemenik Perše, L.; Nanni, F. Advancements in Metal Additive Manufacturing: A Comprehensive Review of Material Extrusion with Highly Filled Polymers. *J. Manuf. Mater. Process.* **2024**, *8*, 14. [CrossRef]
32. Mechter, M.A.; Mace, Y.; Kerbrat, O. A new design for additive manufacturing method: Applied on the bound metal deposition process. *J. Eng. Des.* **2022**, *33*, 787–810. [CrossRef]
33. Mancia, T.; Forcellese, P.; Bellezze, T.; Simoncini, M. Effect of build-up orientation angle and printing speed on mechanical properties and micro- and macro-defect formation in 17-4 PH stainless steel components manufactured by Bound Metal Deposition. *Int. J. Adv. Manuf. Technol.* **2024**, *132*, 4285–4295. [CrossRef]
34. Hartsfield, C.R.; Shelton, T.E.; Cobb, G.R.; Kemnitz, R.A.; Weber, J. Understanding Flow Characteristics in Metal Additive Manufacturing. *J. Aerosp. Eng.* **2021**, *34*, 04021082. [CrossRef]
35. Tao, Y.B.; He, Y.L.; Huang, J. Numerical study of local heat transfer coefficient and fin efficiency of wavy fin-and-tube heat exchangers. *Int. J. Therm. Sci.* **2007**, *46*, 768–778. [CrossRef]
36. Wang, Y.; Chen, C.; Ren, R.; Xue, Z.; Wang, H.; Zhang, Y.; Wang, J.; Wang, J.; Chen, L.; Mu, W. Ferrite formation and decomposition in 316H austenitic stainless steel electro slag remelting ingot for nuclear power applications. *Mater. Charact.* **2024**, *218*, 114581. [CrossRef]
37. Chu, H.-Y.; Shiue, R.-K.; Cheng, S.-Y. The Effect of Homogenization Heat Treatment on 316L Stainless Steel Cast Billet. *Materials* **2024**, *17*, 232. [CrossRef]
38. Suwanpreecha, C.; Songkuea, S.; Linjee, S.; Muengto, S.; Bumrungpon, M.; Manonukul, A. Tensile and axial fatigue properties of AISI 316L stainless steel fabricated by materials extrusion additive manufacturing. *Mater. Today Commun.* **2023**, *35*, 105667. [CrossRef]